Supporting information

Boosting Wide-Temperature Solid-State Lithium Metal Batteries by Polyether-Carbonate Hybridization

Jia Chou[a], Shengbo Yang[a,b], Zhixing Wang[a,b], Huajun Guo[a,b], Xinhai Li[a,b], Guochun Yan[a,b], Guangchao Li[a], Wenjie Peng[a], Zhenghui Liu[c], Jiexi Wang[a,b], Hui Duan*[,a,b]

[a] National Energy Metal Resources and New Materials Key Laboratory, Engineering Research Center of the Ministry of Education for Advanced Battery Materials, Hunan Provincial Key Laboratory of Nonferrous Value-Added Metallurgy, School of Metallurgy and Environment, Central South University, Changsha 410083, P. R. China.

[b] National Engineering Research Centre of Advanced Energy Storage Materials, Changsha, 410205, P. R. China

[c] Department of Chemistry, Taizhou University, Taizhou 318000, Zhejiang, P. R. China.

* Corresponding author, email address: duanhui@csu.edu.cn (H. Duan)

A. Supplementary Methods

1. Materials and Methods

I. Synthesis of poly(1,3-dioxolane)-poly(propylene carbonate)-poly(vinylene carbonate) (poly(DOL)-poly(PC)-poly(VC), or PDPC).

A precursor solution of DOL, PC and VC is prepared with a ratio of 70:25:5. 1 mmol lithium salt lithium bis(trifluoromethanesulfonyl)-imide (LiTFSI) and 1 mmol Lithium difluoro(oxalato) Borate (LiDFOB) as initiator were weighed and added into the solution. After the mixed solution turns to transparent and homogeneous, the precursor solution was coated on electrodes or stayed in bottle for characterizations. All the processes of preparing the SPE were conducted in an Ar-filled glove box. After assembling the batteries and staying for 10 hours at room temperature, solid-state polymer PDPC was obatined through an in-situ cationic ring-opening polymerization approach.

II. Preparation of cathodes and fabrication of batteries.

The cathode slurry was prepared by mixing NCM/$LiFePO_4$, Super P and polyvinylidene difluoride (PVDF) in N-methyl-2 pyrrolidone (NMP) with a mass ratio of 8:1:1, then casted on carbon-coated aluminum foil and dried at 80 °C for 12 h. The CR2032-type coin cells were assembled in an Ar-filled glove box (H_2O<0.1 ppm, O_2<0.1 ppm). The precursor solution was injected into the sandwich structure consisting of cathode, Celgard separator and Li foil. Subsequently, PDPC SPE was polymerized inside the assembled batteries according to the above approach of in-situ polymerization. The coin cells of control group were assembled by the same route, but the electrolyte adopts the classic LE of 1.0 mol·L^{-1} $LiPF_6$ in EC: DEC: DMC with a volume ratio of 1:1:1.

2. Characterizations

^1H, ^7Li and ^{19}F NMR spectra were collected on a Bruker AVANCE II+ 400 MHz with $(CD_3)_2SO$ as deuterated solvent to deduce the structure of polymers. In order to investigate functional groups of polymers, the spectra were recorded using fourier transform infrared spectrometer (FTIR Thermo, Fisher iN10-iZ10) in the range of 400~4000 cm^{-1} and Raman spectra utilizing Thermo Fisher DXR in the range of 200~700 cm^{-1}. The thermal behavior of polymers were analyzed by an apparatus of thermogravimetric analysis (Netzsch STA449F3) at a heating rate of 10 °C min^{-1} from 25°C ~500°C. The crystalline properties of the polymers were measured with the utilize of differential scanning calorimetry (Netzsch DSC214) at a heating rate of 10°C min^{-1} from −100°C to 100°C

under nitrogen atmosphere. The micrographs of lithium anodes in cycled batteries were collected by scanning electron microscopy (SEM, JEOL 6710F) operated at 10kV. The cycled lithium anodes were characterized by X-ray photoelectron spectroscopy (XPS, Thermo Scientific ESCALAB 250Xi).

3. Quantum Chemistry Calculation Details

DFT calculations were performed with Gaussian16 and ORCA 6.0 software package [1]. The geometry optimizations were performed using the B3LYP functional [2] with the Becke-Johnson damping scheme (D3BJ) [3], and the def2-SVP basis [4] was using for all atoms. Energy calculations were performed using the wB97M-V functional [5] with the def2-TZVP basis set [6] for all atoms.

4. Molecular Dynamics (MD) Simulations

The partial charge of LiTFSI，polymer PDPC and PEO molecules were calculated using Gaussian 16 code and the 6-311g(d,p) basis functions were applied [7]. The OPLS-AA force field and Auxiliary Tools of Force Field (AuToFF) were used to parametrize all atoms, such as the bond parameters, angle parameters and the dihedral angles, and so on. The parameters of $TFSI^-$ are derived from OPLS-2009IL force field [8]. The coordination structures of solvents, cations and anions in different electrolytes were simulated by molecular dynamics (MD) simulation. In system 1, the monomer ratio of LiTFSI:PDPC =1:1 and 100 LiTFSI and 100 PDPC molecules were randomly inserted into a cube box with a side length of 8.0 nm; In system 2, the monomer ratio of LiTFSI:PEO =1:2 and 100 LiTFSI and 200 PEO molecules were randomly inserted into a cube box with a side length of 8.0 nm, too. The MD simulations were performed in the GROMACS 2021 software package [9-11]. The steepest descent method was applied to minimize the initial energy for each system with a force tolerance of 1 $kJ/(mol^{-1}\ nm^{-1})$ and a maximum step size of 0.002 ps before MD calculations [12]. In all the three directions, periodic boundary conditions were imposed. Leapfrog algorithm was used to integrate the Newtonian equation of motion. The MD simulation was processed in an NPT ensemble and the simulation time is 20 ns. In NPT simulations, the pressure was maintained at 1 bar by the Berendsen barostat in an isotropic manner [13-15] and the temperature was maintained by the V-rescale thermostat at 298.15 K. The LINCS algorithm [16] was performed for constrain bond lengths of hydrogen atoms. A cutoff of 1.2 nm was employed to calculate the short-range van der Waals interactions and electrostatic interactions .The density

functional theory (DFT) calculations were performed in Vienna *ab initio* Simulation package (VASP). The projector augmented-wave (PAW) pseudopotentials and Perdew-Burke-Ernzerhof(PBE) generalized-gradient approximation (GGA) functional were adopted in all DFT calculations. Particularly, the van der Walls (vdW) interaction was described with DFT-D3 method as physical interaction takes an important role when considering the adsorption. The energy cutoff was set to 400 eV. Besides, the self-consistent field (SCF) and geometry convergence tolerance were set to 1×10^{-5} and 1×10^{-4} eV, respectively.

5. Electrochemical performance tests

The electrochemical impedance spectroscopy (EIS) measurements were performed on a Princeton PARSTAT MC 1000 multi-channel electrochemical workstation over the frequency ranging from 0.1 Hz to 100 kHz with an amplitude of 10 mV. The conductivity of SPE was calculated by following equation: $\sigma = d / SR$, where d was the distance between two stainless steel plates, R is the impedance resistance measured by EIS, and S was the effective contact area. The conductivities (σ) under different temperatures from -10°C to 60°C of the SS/SPE/SS models were applied to calculate the activation energy (Ea), according to the Arrhenius law ($\sigma = A \exp(-Ea/RT)$), (A: frequency factor, R: molar gas constant, T:absolute temperature). The chronoamperometry test was used to evaluate the Li ion transference number on the Li|PDPC|Li models with the applied voltage of 0.01 V. Before and after the chronoamperometry test, the impedance resistance was measured by EIS. The galvanostatic charge/discharge tests of batteries with PDPC SPE and LE were examined on LAND testing system (LANHE CT2001A). Linear sweep voltammetry (LSV) analysis was conducted in Li||SS cell from 2.2 V to 6.0 V at a scan rate of 0.5 mV s^{-1}. Li ion transference number (t_{Li^+}) was measured using the constant potential polarization method.[17] A small polarization potential (ΔV) of 10 mV was applied to symmetric Li|SPE|Li cell. The value of t_{Li^+} was calculated from the following equation: $t_{Li^+} = [(\Delta V - I_0R_0)]/[I_0 (\Delta V - I_{ss}R_{ss})]$. I_{ss} and I_0 are the steady and initial currents, while R_{ss} and R_0 are the steady and initial interfacial resistance, respectively.

B. Supplementary Figures

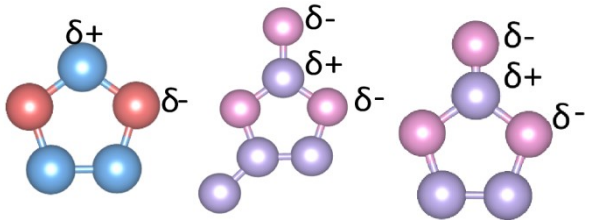

Fig. S1. The optimized geometric configurations of monomers DOL, PC and VC.

Fig. S2. The polymerization mechanism of cationic ring-opening polymerization of PDOL and VC or PC. DOL served as the electron-donor, while DOL, VC or PC served as electron-acceptor.

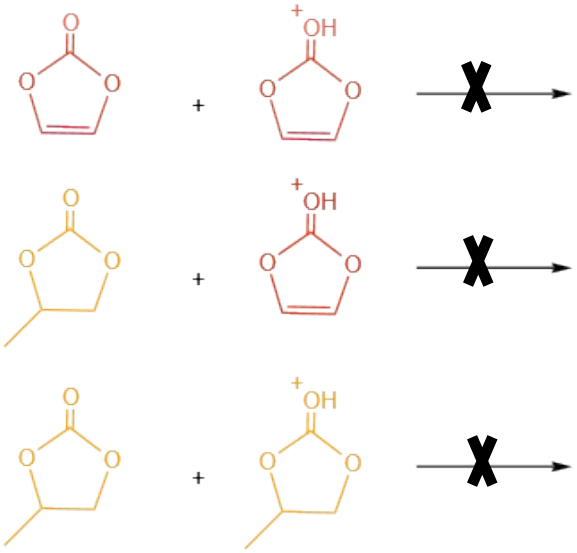

Fig. S3. The cationic ring-opening polymerization reactions which could not happen between VC and PC.

Fig. S4. Optical images of PDPC SPE in-situ synthesized in a bottle.

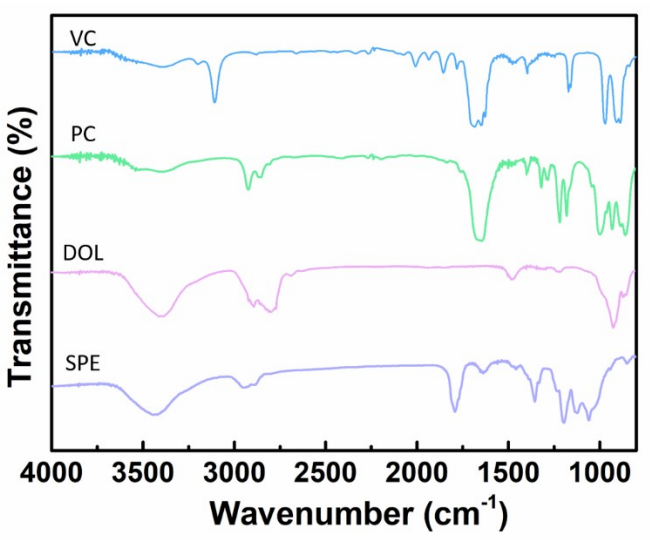

Fig. S5. Fourier Transform Infrared Spectroscopy (FT-IR) spectrum of the monomer VC, PC, DOL and SPE. The peaks of polymers were assigned as follows: -C-H- stretching vibration of alkene carbon (3100-3010 cm^{-1}), -C-H- of saturated carbon stretching vibration (2960–2850 cm^{-1}), -C=O stretching vibration of cyclic carbonate anhydride (1710-1860 cm^{-1}), -C=C- stretching vibration (1687-1600 cm^{-1}), -C-O-C- stretching vibration (1300-910 cm^{-1}), -C-C(=O)-O- stretching vibration of saturated carbonate (1210-1163 cm^{-1}) and -C=O- stretching vibration of saturated carbonate (1750-1735 cm^{-1}).

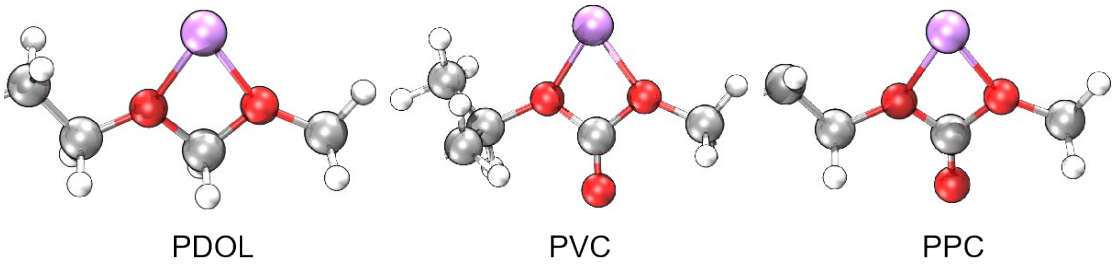

Fig. S6. The binding configuration of PDOL, PPC and PVC fragments with Li^{+}.

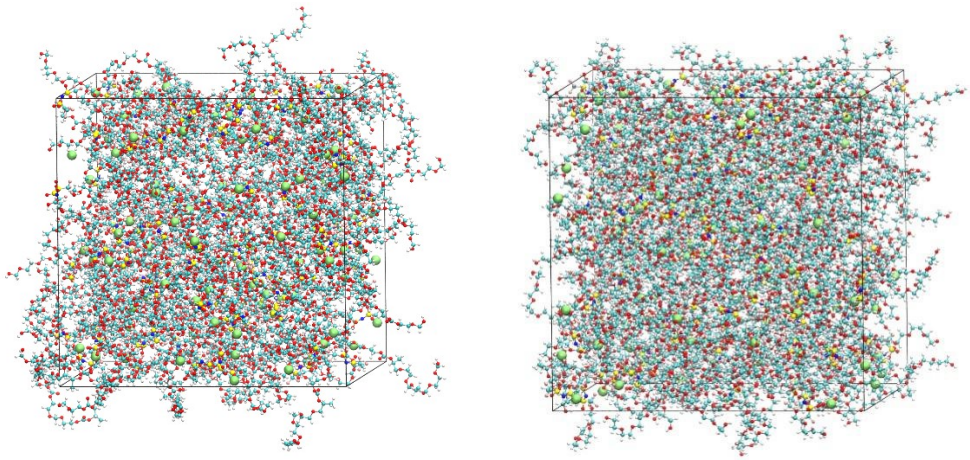

Fig. S7. (a) Snapshot of MD simulation of solid polymer electrolyte PDPC. **(b)** Snapshot of MD simulation of solid polymer electrolyte PEO.

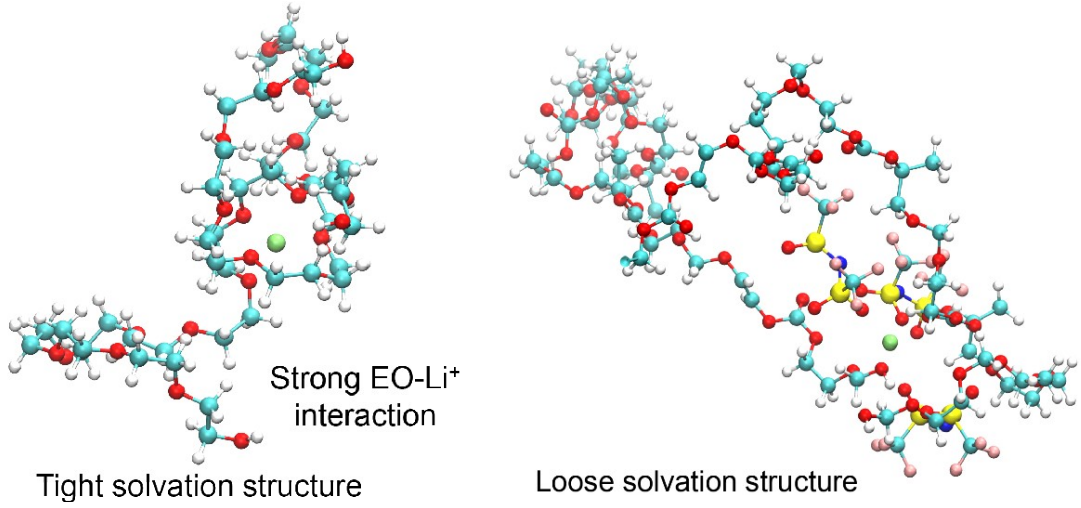

Fig. S8. Coordination structure of solid polymer electrolyte PEO and PDPC.

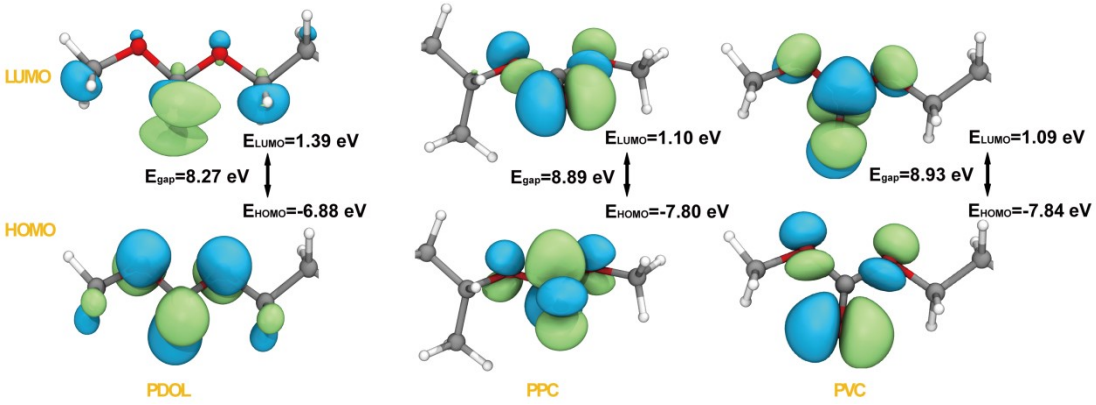

Fig. S9. The HOMO and LUMO energy levels of PDOL, PPC and PVC fragments.

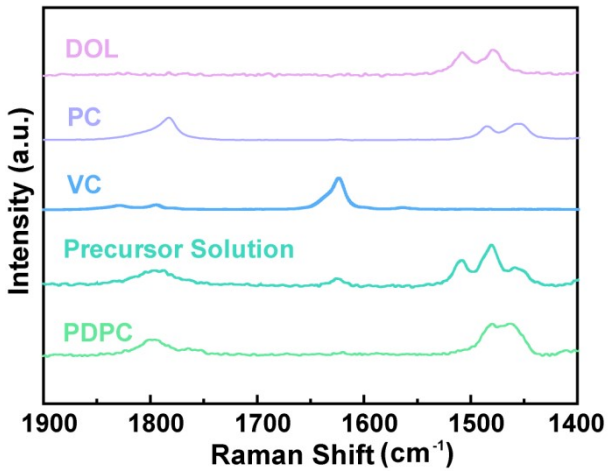

Fig. S10. Raman spectra of DOL, PC, VC, precursor solution and PDPC from 1400 cm^{-1} to 1900 cm^{-1}.

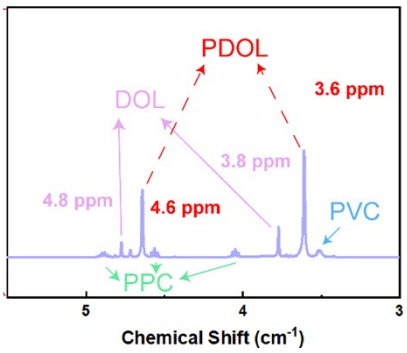

Fig. S11. ^{1}H NMR spectra of PDPC, VC, PC and DOL and its locally enlarged view of PDPC. Quantitative integration of ^{1}H NMR spectra reveals that 87% of the DOL monomer has polymerized. Since DOL constitutes 70% of the total precursor solution, the residual liquid content in the in-situ polymerized PDPC SPE is calculated to be 9% (70%×13% unreacted DOL).

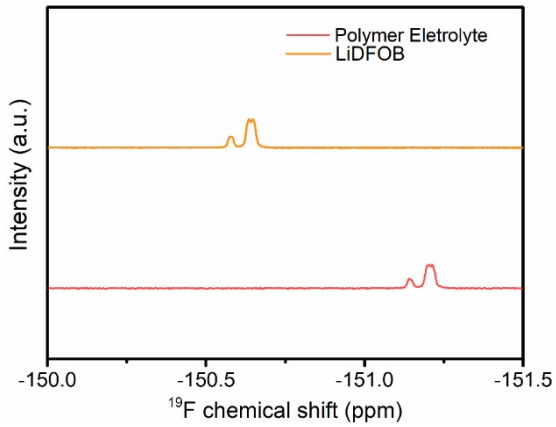

Fig. S12. ^{19}F NMR spectra of LiDFOB and PDPC SPE.

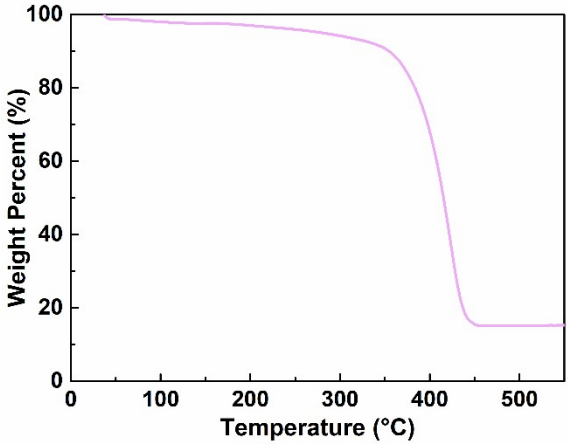

Fig. S13. Thermogravimetric analysis (TGA) curve of PDPC SPE.

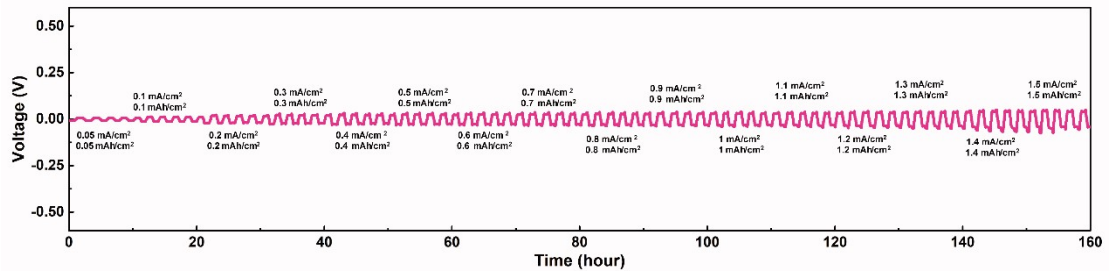

Fig. S14. Galvanostatic Li plating/stripping voltage profiles at step-increased current densities of Li/Li symmetric cells from 0.05 mA cm^{-2} to 1.5 mA cm^{-2} assembled with the PDPC SPE.

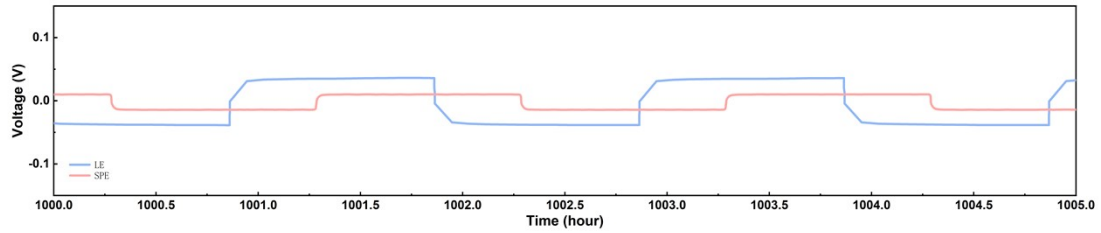

Fig. S15. The locally enlarged view of curves of Li/PDPC/Li and Li/LE/Li symmetrical cells with the current densities of 0.2 mA cm^{-2} for 0.2 mAh cm^{-2}.

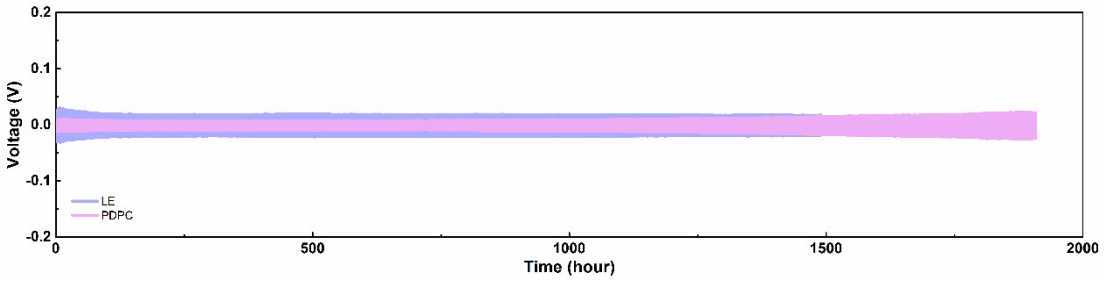

Fig. S16. The curves of Li|PDPC|Li and Li|LE|Li symmetrical batteries with the current densities of 0.1 mA cm^{-2} for 0.1 mAh cm^{-2} at 25°C.

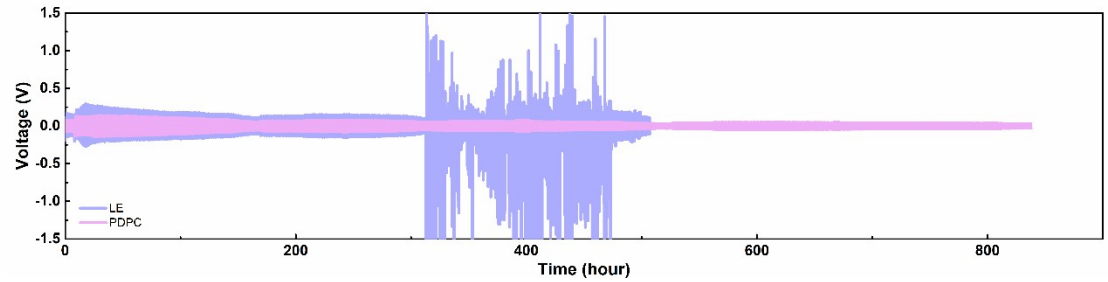

Fig. S17. The curves of Li|PDPC|Li and Li|LE|Li symmetrical batteries with the current densities of 0.05 mA cm^{-2} for 0.05 mAh cm^{-2} at -10°C.

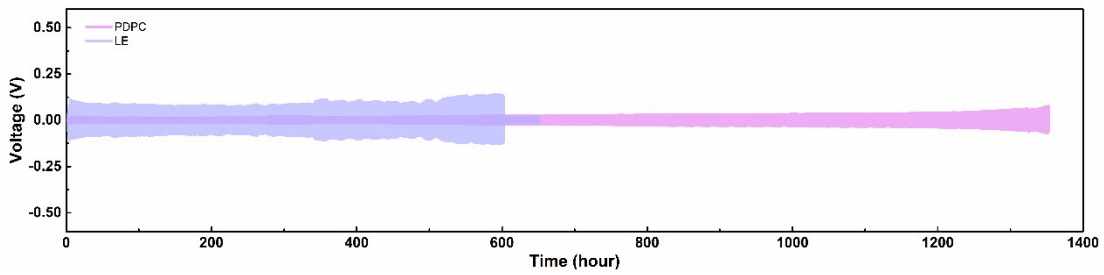

Fig. S18. The curves of Li|PDPC|Li and Li|LE|Li symmetrical batteries with the current densities of 0.2 mA cm^{-2} for 0.2 mAh cm^{-2} at 60°C.

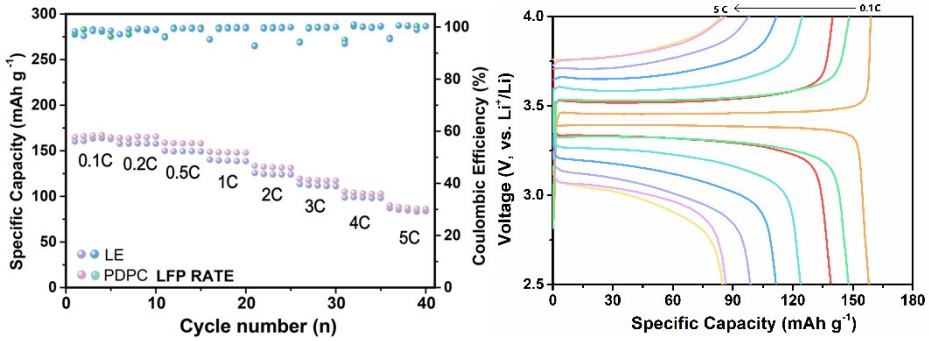

Fig. S19. The rate performance of Li/PDPC/LFP and Li/LE/LFP batteries at different rates of 0.1, 0.2, 0.5, 1, 2, 3, 4, and 5 C. The corresponding charge/discharge curves of Li/LE/LFP batteries at different rates of 0.1, 0.2, 0.5, 1, 2, 3, 4, and 5 C.

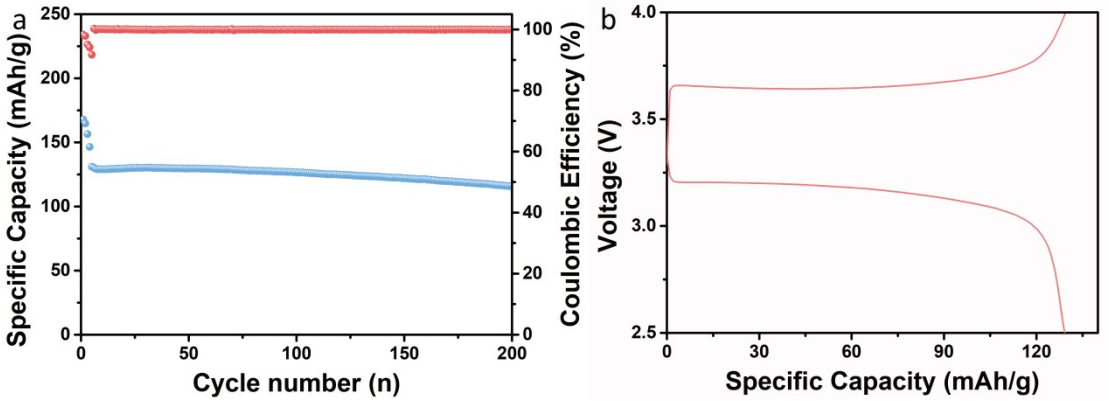

Fig. S20. The cycling performance and the corresponding charging/discharging curve of Li|PDPC|LFP battery at 2 C.

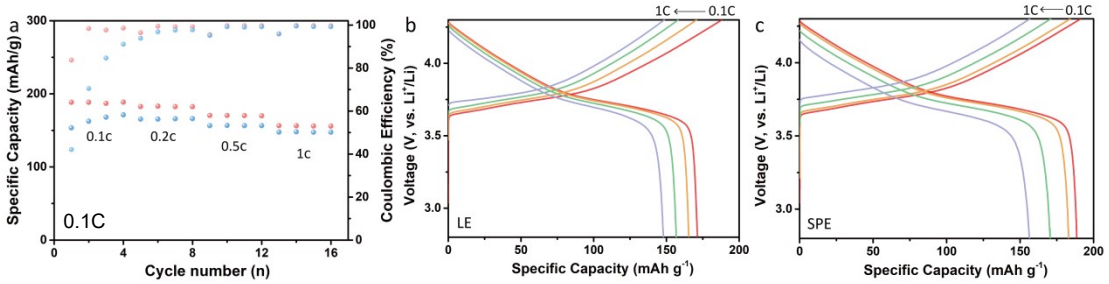

Fig. S21. The rate performance and the corresponding charging/discharging curves of

NCM523|SPE|Li batteries and NCM523|LE|Li batteries at different rates of 0.1 C, 0.2 C, 0.5 C and 1 C. (Red dots represent PDPC, and the blue dots represent LE)

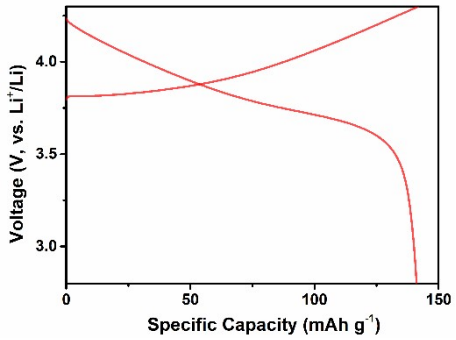

Fig. S22. The corresponding charging/discharging curves of NCM523|SPE|Li battery at 1 C.

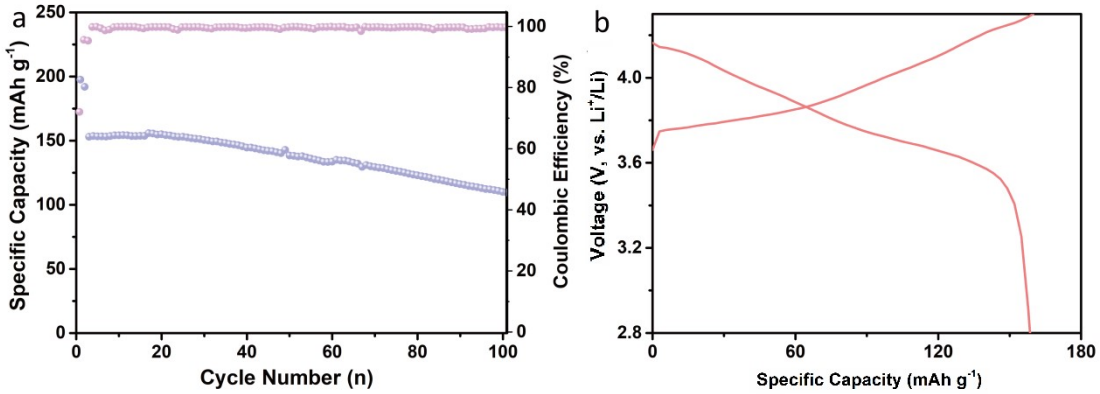

Fig. S23. The cycling performance and the corresponding charging/discharging curve of NCM811|SPE|Li battery at 0.5 C.

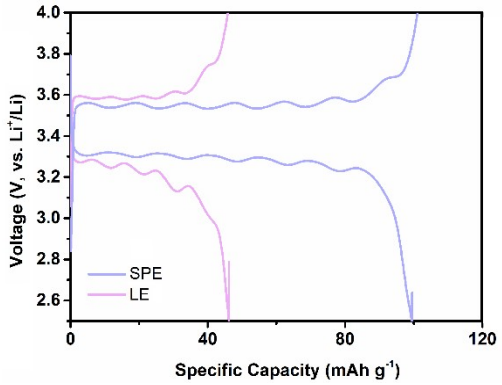

Fig. S24. The charging/discharging curves of Li|PDPC|LFP battery and Li|LE|LFP battery at 1 C and -10 °C.

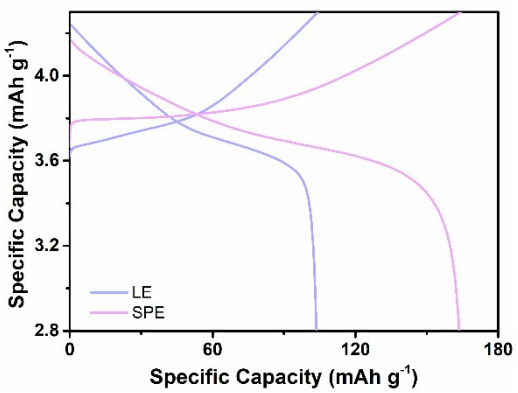

Fig. S25. The charging/discharging curves of Li|PDPC|NCM523 battery and Li|LE|NCM523 battery at 1 C and 60 °C.

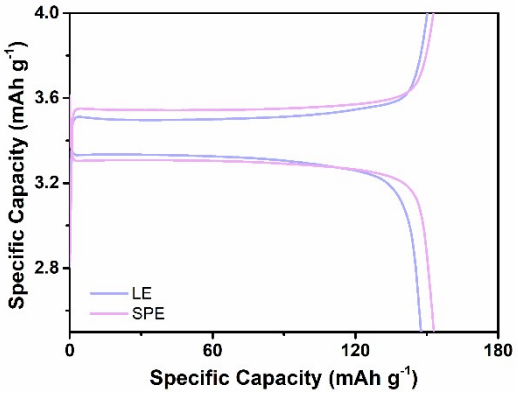

Fig. S26. The charging/discharging curves of Li|PDPC|LFP battery and Li|LE|LFP battery at 1 C and 60 °C.

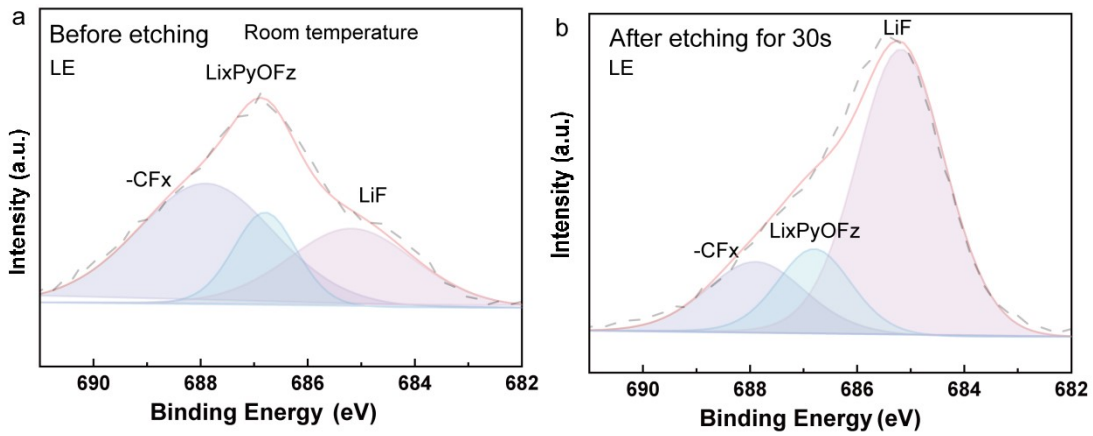

Fig. S27. XPS depth profiling spectra for C element of cycled Li-LFP batteries with LE electrolyte at 25˚C.

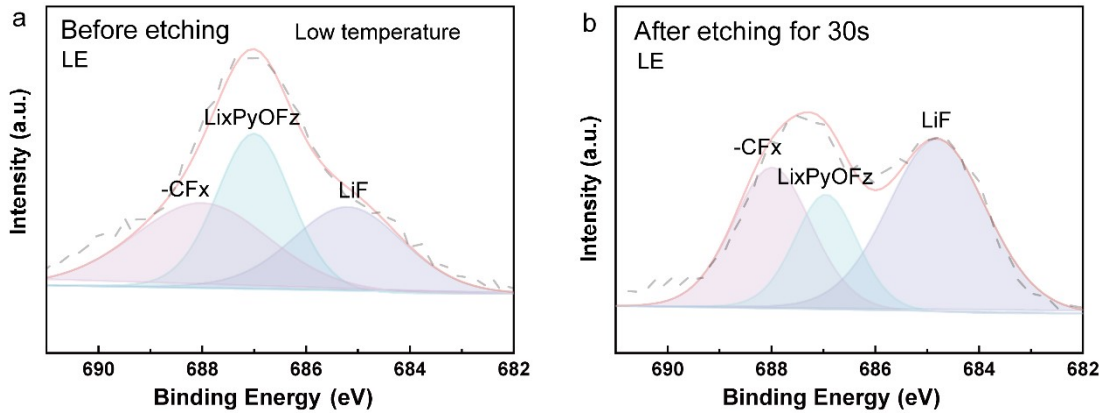

Fig. S28. XPS depth profiling spectra for C element of cycled Li-LFP batteries with LE electrolyte at -10˚C.

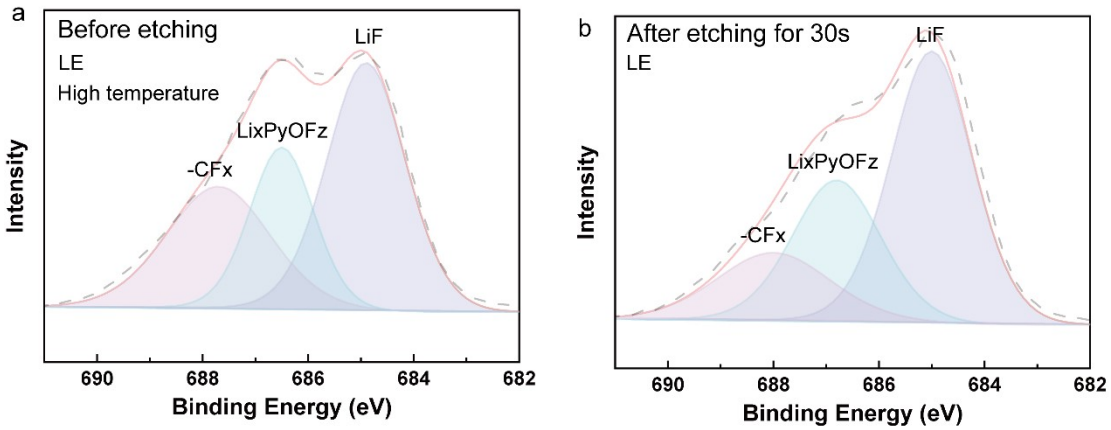

Fig. S29. XPS depth profiling spectra for C element of cycled Li-LFP batteries with LE electrolyte at 60˚C.

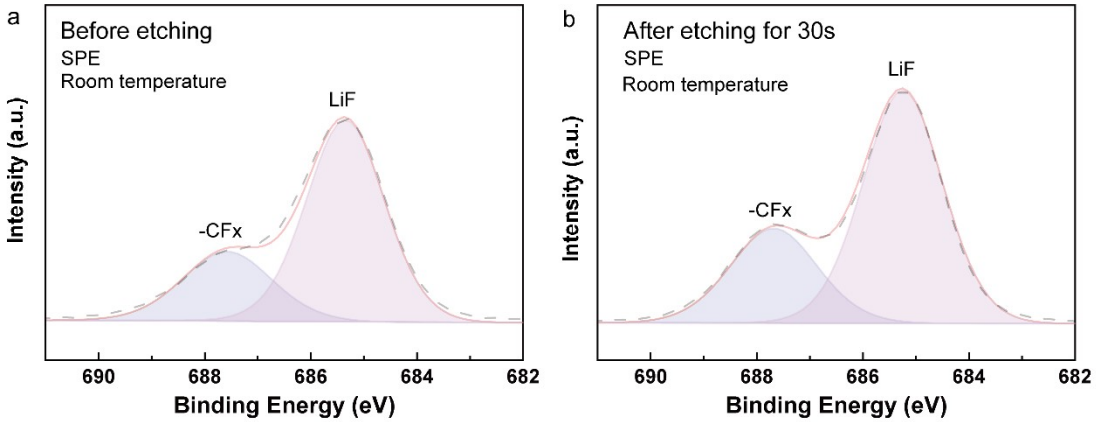

Fig. S30. XPS depth profiling spectra for F element of cycled Li-LFP batteries with PDPC electrolyte at 25 ˚C.

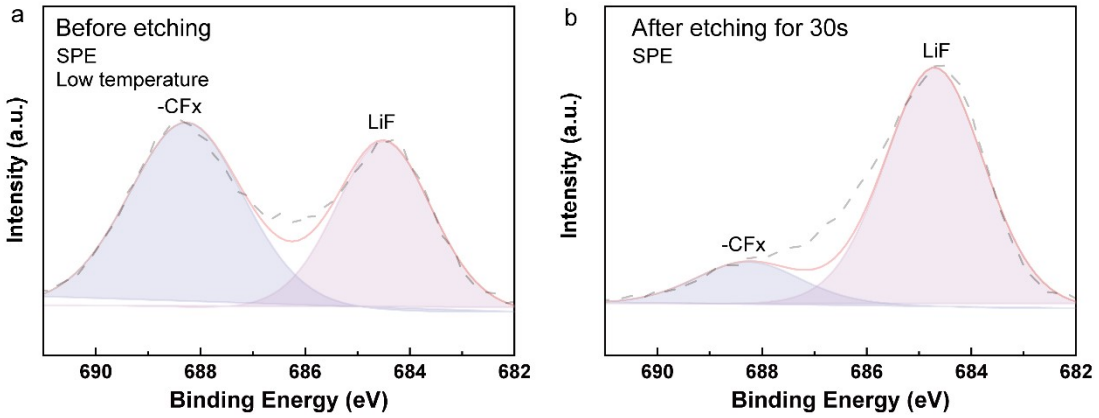

Fig. S31. XPS depth profiling spectra for C element of cycled Li-LFP batteries with PDPC electrolyte at -10 ˚C.

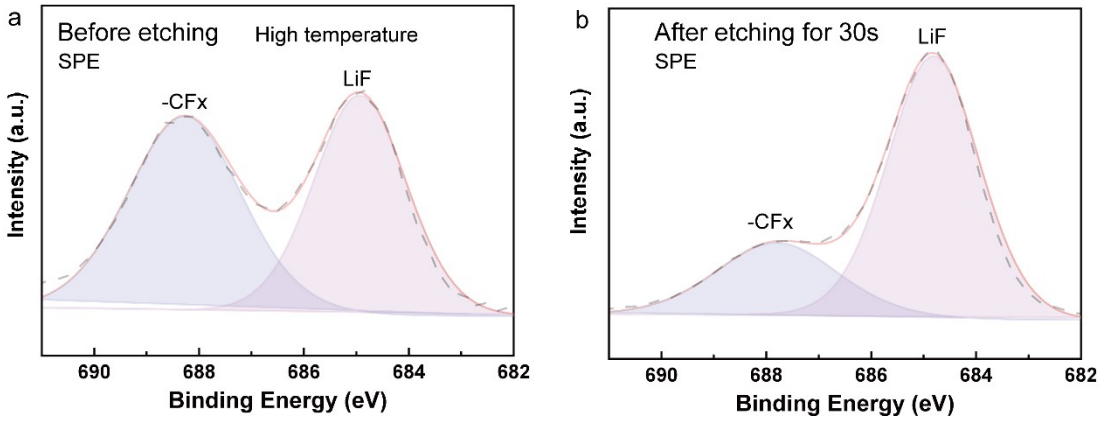

Fig. S32. XPS depth profiling spectra for C element of cycled Li-LFP batteries with PDPC electrolyte at 60 ˚C.

Supplementary Tables

Table S1. Simulated experiment in bottles to investigate the feasibility of monomer polymerization.

Number	Monomers	Functional Groups	Phenomena	Conclusion
1	Allyl Glycidyl Ether	Allyl, epoxy group	 High-viscosity liquid state.	Incomplete Polymerization.
2	1,4-Dioxane	oxirane group	 Viscous white suspension.	Incomplete Polymerization.
3	Ethylene Carbonate	Lactone group	 Liquid state.	Polymerization Failure.

Not all ether and carbonate monomers are compatible with the in-situ synthesis approach based on cationic ring-opening reaction. This method typically requires monomers with electron-rich groups (electron-donors) or electron-deficient groups (electron-acceptors), including oxetanes and lactones with enough reactivities.

Table S2. Comparison of this work which exhibits excellent capacity with other studies for wide-temperature Li-LFP batteries by recent references.

SPE	Temperature (°C)	Initial capacity (mAh g^{-1})	Rate	Reference
PDPC	**25**	**148**	**1 C**	***This work***
	-10	**127**	**0.1 C**	
	60	**140**	**1 C**	
Li-HA-F CSE	25	139	0.2 C	*Journal of the American Chemical Society* [18]
	-10	58	0.2 C	
	60	142	0.2 C	
PDSE	30	138	0.1 C	*Advanced Energy Materials*[19]
	-10	74	0.1 C	
	50	158	0.1 C	
ASPE	25	125	1 C	*Advanced Materials*[20]
	-20	105	0.2 C	
D-QSPE	25	130	1 C	*Energy Storage Materials, 2024*[21]
	-20	82	0.1 C	
	60	126	1 C	
DSPE	20	138	1 C	*Energy Storage Materials, 2021*[22]
	-10	61	0.1 C	
	60	160	0.1 C	
CPE	25	148	0.5 C	*Nano energy*[23]
	-10	108	0.1 C	
	60	142	0.5 C	

D. Supplementary References

[1] (A) Gaussian 16, Revision A.01, M. J. Frisch, G. W. Trucks, et al, Gaussian, Inc., Wallingford CT, **2016**. https://gaussian.com. (B) Neese F. The ORCA program system[J]. Wiley Interdisciplinary Reviews: Computational Molecular Science, **2012**, 2(1): 73-78. (C) Neese F, Wennmohs F, Becker U, et al. The ORCA quantum chemistry program package[J]. The Journal of chemical physics, **2020**, 152(22).

[2] Becke A D. Density-functional exchange-energy approximation with correct asymptotic behavior[J]. Physical review A, **1988**, 38(6): 3098.

[3] (A) S.Grimme, S.Ehrlich, L.Goerigk, J Comput Chem, **2011**, 32, 1456–1465. (B) S.Grimme, J.Antony, S.Ehrlich and H.Krieg, J.Chem.Phys., **2010**, 132, 154104.

[4] F. Weigend and R. Ahlrichs, Phys. Chem. Chem. Phys. **2005**, 7, 3297.

[5] N. Mardirossian and M. Head-Gordon., J. Chem. Phys. **2016**, 144, 214110.

[6] (A) F. Weigend, R. Ahlrichs Phys. Chem. Chem. Phys. **2005**, 7 3297. (B) J. Zheng, X. Xu, and D. G. Truhlar Theor. Chem. Acc. **2010**, 128, 295-305.

[7] G.A. Petersson, M.A. Al-Laham, A complete basis set model chemistry. II. Open-shell systems and the total energies of the first-row atoms, J. Chem. Phys. **1991**, 94, 6081–609.

[8] Doherty, Brian and Zhong, Xiang and Gathiaka, Symon and Li, Bin and Acevedo, Orlando. Revisiting OPLS Force Field Parameters for Ionic Liquid Simulations. Journal of Chemical Theory and Computation, **2017**, 12(13): 6131-6145.

[9] Spoel D V D, Lindahl E, Hess B, et al. GROMACS: fast, flexible, and free[J]. Journal of Computational Chemistry, **2005**, 26(16): 1701-1718.

[10] Abraham, et al. GROMACS: high performance molecular simulations through multi-level parallelism from laptops to supercomputers, Software X. **2015**, 1 (2), 19–25.

[11] H.J.C. Berendsen, D. van der Spoel, R. van Drunen,GROMACS: A message-passing parallel molecular dynamics implementation,Comp. Phys. Comm., **1995**, 91, 43-56.

[12] Van Gunsteren, W. F.; Berendsen, H., A leap-frog algorithm for stochastic dynamics. Mol. Simul. **1988**, 1 (3), 173-185

[13] Hess, B.; Bekker, H.; Berendsen, H. J.; Fraaije, J. G., LINCS: a linear constraint solver for molecular simulations[J]. J. Comput. Chem. **1997**, 18 (12), 1463-1472.

[14]Uehara, S.; Hanasaki, I.; Arai, Y.; Nagai, T.; Kawano, S. Statistical Characterisation of Single-Stranded DNA Motion near Glass Surface Beyond Diffusion Coefficient. Micro Nano Lett. **2014**, 9, 257−260.

[15] Humphrey, W.; Dalke, A.; Schulten, K. VMD: Visual Molecular Dynamics. J. Mol. Graphics **1996**, 14, 3 3−38.

[16] Hess, B.; Bekker, H.; Berendsen, H. J.; Fraaije, J. G., LINCS: a linear constraint solver for molecular simulations[J]. J. Comput. Chem. **1997**, 18 (12), 1463-1472.

[17] K. M. Abraham, Z. Jiang, B. Carroll, Chem. Mater. **1997**, 9, 1978.

[18] Jiaying Peng, Dawei Lu, Shiqi Wu, Na Yang, Yujie Cui, Zhaokun Ma, Mengyue Liu, Yongzheng Shi, Yilin Sun*, Jin Niu*, Feng Wang*, J. Am. Chem. Soc., **2024**, 146, 17, 11897–11905.

[19] Wenjie Ren, Xinchao Shang, Yan Lin, Hao Ren, Linchen Zhang, Hang Su, Qi Li, Linjie Zhi, Mingbo Wu, and Zhongtao Li*, Adv. Energy Mater., **2024**, 2405284.

[20] Yuhan Liu, Pinhui Wang, Zhenyue Yang, Liying Wang, Zhangnan Li, Chengzhe Liu, Baijun Liu, Zhaoyan Sun, Hanwen Pei, Zhongyuan Lv, Wei Hu, Yunfeng Lu, Guangshan Zhu*, Adv. Mater., **2024**, 36, 2400970.

[21] Yayue He, Xinyuan Shan, Yue Li, Zhenxi Li, Lin Li, Sheng Zhao, Shilun Gao, Jiali Qu, Huabin Yang, Peng-Fei Cao*, Energy Storage Mater., **2024**, 68, 103281.

[22] Jing Yu, Liu, Jiapeng Liu, Xidong Lin, Ho Mei Law, Guodong Zhou, Stephen C. T. Kwok, Matthew J. Robson, Junxiong Wu, Francesco Ciucci*, Energy Storage Mater., **2021**, 37, 609.

[23] Jin Li, Yingjun Cai, Yingyue Cui, Hui Wu, Haoran Da, Yijun Yang, Haitao Zhang, Suojiang

Zhang*, Nano Energy, **2022**, 95, 107027.